Engineering Fracture Mechanics 252 (2021) 107792

Contents lists available at ScienceDirect

Engineering Fracture Mechanics

journal homepage: www.elsevier.com/locate/engfracmech

Mixed-mode cohesive laws and the use of linear-elastic fracture mechanics

S. Goutianos [a,*], B.F. Sørensen [b], M.D. Thouless [c]

[a] Department of Manufacturing and Civil Engineering, Norwegian University of Science and Technology, Teknologivegen 22, 2815 Gjøvik, Norway

[b] Department of Wind Energy, Section of Composite Mechanics and Structures, Technical University of Denmark, Risø Campus, DK 4000, Roskilde, Denmark

[c] Department of Mechanical Engineering, Department of Materials Science & Engineering, University of Michigan, Ann Arbor, MI 48109-2125, USA

ARTICLE INFO

Keywords:
Mixed-mode
Cohesive zone models
Phase angle
Linear-elastic fracture mechanics

ABSTRACT

Small-scale cohesive-zone models based on potential functions are expected to be consistent with the important features of linear-elastic fracture mechanics (LEFM). These include an inverse-square-root K-field ahead of a crack, with the normal and shear stresses being proportional to the mode-I and mode-II stress-intensity factors, K_I and K_{II}, the work done against crack-tip tractions being equal to $\left(K_I^2 + K_{II}^2\right)/\bar{E}$, where $\bar{E}$ is the appropriate modulus, and failure being controlled by the toughness. The use of an LEFM model also implicitly implies that the partition of the crack-tip work into shear and normal components is given by a phase angle defined as $\psi_K = \tan^{-1}\left(K_{II}/K_I\right)$. In this paper, we show that the partition of crack-tip work in a cohesive-zone model is consistent with LEFM if the normal and shear deformations across an interface are uncoupled. However, we also show that this is not the case for coupled cohesive laws, even if these are derived from a potential function. For coupled laws, LEFM cannot be used to predict the partition of work at the crack tip even when the small-scale requirements for LEFM conditions being met; furthermore, the partition of the work may depend on the loading path. This implies that LEFM cannot be used to predict mixed-mode fracture for interfaces that are described by coupled cohesive laws, and that have a phase-angle-dependent toughness.

1. Introduction

Cohesive-zone models, originating from the work of Hillerborg et al. [1] and Needleman [2], are widely used to simulate the initiation and growth of cracks in problems ranging from the materials scale [2–5] to the structural scale, such as adhesive joints [6–8] and wind turbine blades [9]. In these models, the fracture process is described by a traction–separation relationship, known as a cohesive law, that comprises both a strength (peak traction) and a fracture energy (area under the traction–separation curve) [10,11]. The use of cohesive laws allows a transition between the strength-based approach to fracture of [12] and the energy-based method of [13] that underpins linear-elastic fracture mechanics (LEFM) [14–16].

Since [17] and [18] generalized cohesive laws to include shear tractions, cohesive-zone modelling has been extended to mixed-mode fracture, with many different cohesive laws being developed. These cohesive laws can be divided into several fundamentally different groups [19]. First, there are those derived from potential functions, and those that are not derivable from potential functions. Second, there are what are termed as "uncoupled" and "coupled" mixed-mode laws.

* Corresponding author.
E-mail address: stergios.goutianos@ntnu.no (S. Goutianos).

https://doi.org/10.1016/j.engfracmech.2021.107792
Received 30 June 2020; Received in revised form 26 March 2021; Accepted 12 May 2021
Available online 18 June 2021

Potential-based cohesive laws are independent of the loading history. The normal and shear tractions depend only on the values of the normal and tangential openings; they do not depend on the path by which those openings are reached. As an example, micromechanical modelling can be used to show that cross-over fibre-bridging gives coupled laws for which a potential function exists [20]. For cohesive laws that cannot be derived from a potential function, the cohesive tractions and the work of the cohesive tractions depend on the loading path. Such laws can be used to model fracture processes that include history-dependent phenomena such as plasticity or frictional sliding [21]. However, attention is focused in this paper on conditions that might be consistent with LEFM, so only potential-based cohesive laws are considered in the present work; history-dependent mechanisms are excluded.

In "uncoupled" mixed-mode cohesive laws, the normal tractions depend only on the normal openings, and the shear tractions depend only on the tangential (shear) openings. However, despite the terminology, coupling between the two modes of deformation is inherently introduced through the failure criterion [22]. This coupling generally manifests itself as a relationship between the critical normal and shear displacements. In particular, shear decreases the critical opening-displacement, and opening decreases the critical shear displacement. More details are given in Appendix. In coupled cohesive laws, the normal and shear tractions each depend on both the normal and tangential openings. It is not necessary to describe an additional mixed-mode failure criterion with such coupled laws, but the coupling should be consistent with any observed mixed-mode failure criterion.

Under small-scale conditions, the driving force for crack growth in an elastic body is the gradient of total potential energy of the system with respect to the length of the traction-free portion of the crack [23]. In linear-elastic fracture mechanics (LEFM), this is designated by the energy-release rate, $\mathcal{G}$ [13], which is identical to the value of the J-integral taken around the crack tip [23]. Fracture occurs when $\mathcal{G} = \Gamma$, which is identified as the toughness, and is considered to be a material property. Mixed-mode fracture in an LEFM framework is described in terms of the mode-I and mode-II stress-intensity factors, K_I and K_{II}: the amplitudes of the singular normal and shear stresses in the K-dominant region near the crack tip. A phase angle describes the ratio between these two parameters as $\psi_K = \tan^{-1}\left(K_{II}/K_I\right)$, and the toughness is assumed to be a unique function of the phase angle, $\Gamma\left(\psi_K\right)$ [24,25]. Crack growth occurs when $\mathcal{G} = \Gamma(\psi_K)$, where the phase angle describes the ratio K_{II}/K_I at fracture. Two implicit assumptions of LEFM are that the work at the crack tip, and its partition into shear and normal components are both path-independent i.e., independent of whether K_I and K_{II} are applied proportionally (simultaneously) or non-proportionally (e.g. sequentially).

The use of LEFM is predicated on the assumption that any portion of a body not described as a continuum elastic medium is limited to a very small region near the crack tip, and that the macroscopic response of the body is linear-elastic. The use of LEFM as a powerful quantitative tool that is ubiquitous in engineering design is not predicated on singular stresses actually existing at the crack tip, but rather on the fact that the fracture process at the crack tip is dependent only on a macroscopic description of the K-field [26]. In other words, the crack tip (and its partition) are uniquely defined by K_I and K_{II}, and independent of the cohesive length, provided this latter parameter is small enough. The implication of this is that any loading-path dependence that might exist for deformation of the crack tip potentially is inconsistent with the assumptions that underpin the use of LEFM.

In the present study, we investigate this specific issue within the broad framework of small-scale fracture that is generally taken to correspond to LEFM conditions. It is emphasized again that for a fracture problem to be described by LEFM merely requires a small-scale cohesive zone. It does not require singular stresses to actually exist at the crack tip. This has been demonstrated by appropriate small-scale cohesive-zone analyses [16,27,28]. In this paper, we use small-scale cohesive-zone models with potential-based cohesive laws to satisfy one obvious requirement of path-independence, and examine whether there are additional constraints on traction–separation laws for them to provide path-independent, mixed-mode behaviour. In particular, we are interested in whether there may be limitations on when an LEFM framework might be valid to describe small-scale fracture with uncoupled and coupled, potential-based, mixed-mode cohesive laws.

2. Basic mechanics

2.1. Work of cohesive tractions

The local work done (per unit area) against cohesive tractions across a small element of the interface, $\mathcal{W}$, can be decomposed into the local work done against normal tractions (designated as mode-I), $\mathcal{W}_n$, and the local work done against shear tractions (designated as mode-II), $\mathcal{W}_t$:

$$\mathcal{W} = \mathcal{W}_n + \mathcal{W}_t = \int_0^{\delta_n} \sigma_n(\delta_n', \delta_t')d\delta_n' + \int_0^{\delta_t} \sigma_t(\delta_n', \delta_t')d\delta_t' \,, \tag{1}$$

where σ_n and σ_t are the normal and shear tractions, δ_n and δ_t are the normal and shear displacements. Under pure mode-I conditions ($\delta_t = 0$), local failure of the interface occurs when $\delta_n = \delta_{n_c}$, where δ_{n_c} is the normal displacement at failure. This corresponds to $\mathcal{W}_n = \Gamma_n$, which is defined as the mode-I toughness. Under pure mode-II conditions ($\delta_n = 0$), local failure of the interface occurs when $\delta_t = \delta_{t_c}$, where δ_{t_c} is the shear displacement at failure. This corresponds to $\mathcal{W}_t = \Gamma_t$, which is defined as the mode-II toughness.

Of particular interest in fracture mechanics is the work done against the tractions at a cohesive crack tip (defined as the point at which the active cohesive zone ends, $x_1 = 0$ in Fig. 1). The normal and shear displacements at the cohesive crack tip are designated by δ_{n_o} and δ_{t_o}, and the two terms for the work done against the corresponding tractions at this location are designated by $\mathcal{W}_{n_o}$ and $\mathcal{W}_{t_o}$. When the J-integral [29] is evaluated along the cohesive zone out to a region where $\mathcal{W} = 0$, its value is given by [30]:

$$J_{loc} = \mathcal{W}_o = \mathcal{W}_{n_o} + \mathcal{W}_{t_o} = \int_0^{\delta_{n_o}} \sigma_n(\delta_n, \delta_t)d\delta_n + \int_0^{\delta_{t_o}} \sigma_t(\delta_n, \delta_t)d\delta_t = \Phi(\delta_{n_o}, \delta_{t_o}) \,, \tag{2}$$

where $\Phi(\delta_n, \delta_t)$ is the potential function used for the traction–separation law.

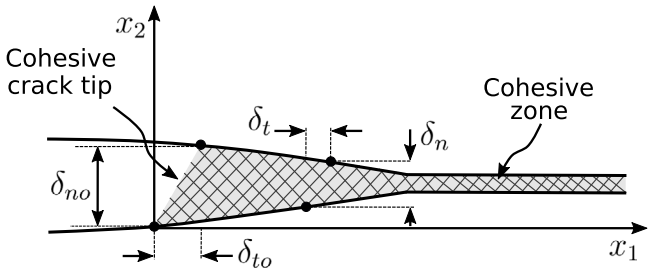

Fig. 1. Definitions of a cohesive crack tip and the associated parameters for the cohesive-zone model. The total opening at the crack tip is $\delta_o = \sqrt{\delta_{no}^2 + \delta_{to}^2}$.

In this paper, the concept of an *instantaneous cohesive length* at the tip of the cohesive crack [16,28] is used. This can be defined for a homogeneous system in modes I and II as

$$\xi_{n_o} = \bar{E}\delta_{n_o}^2/\mathcal{W}_{n_o},\ \xi_{t_o} = \bar{E}\delta_{t_o}^2/\mathcal{W}_{t_o},\ \text{and}\ \xi_o = \bar{E}\delta_o^2/\mathcal{W}_o \tag{3}$$

where $\bar{E} = E/(1-\nu^2)$ in plane strain, $\bar{E} = E$ in plane stress, and E and ν are Young's modulus and Poisson's ratio. These are slightly different from similar quantities defined in terms of the *failure parameters* [1,16,31]. They have the advantages that they can be used to describe the state of the cohesive zone at any stage of loading, and they can be defined for coupled cohesive laws.

The cohesive lengths can be normalized by a characteristic dimension of the geometry, such as a layer thickness, h, so that $\tilde{\xi}_o = \xi_o/h$. If $\tilde{\xi}_o$ is very small, one is in a small-scale regime, and the principles of LEFM are expected to apply. In particular, this means that there will be a K-dominant region ahead of the cohesive crack tip, where the stresses across the interface follow an inverse square-root relationship with respect to distance from the tip, x_1. In the absence of a modulus mismatch across the interface, the normal tractions and shear tractions along x_2 will be described in this region by:

$$\sigma_n = \frac{K_I}{\sqrt{2\pi x_1}};\ \sigma_t = \frac{K_{II}}{\sqrt{2\pi x_1}} \tag{4}$$

where K_I and K_{II} are the mode-I and mode-II stress-intensity factors. Close to the crack tip, the stresses will deviate from this relationship, with the details of the stress field being dependent on the cohesive law. Beyond the K-dominant region, the stresses will deviate from this relationship, following the non-singular, elastic, stress field of the structure. The region over which the K-field describes the stresses may be very small; however such a region will exist if $\tilde{\xi}_o$ is small enough. Again, we emphasize that a central tenet of LEFM is that it can be used to describe fracture if $\tilde{\xi}_o$ is small, it does not have to be zero. It is for this reason that cohesive-zone models can be used to describe LEFM under small-scale conditions [16,27,28].

Under LEFM conditions, an evaluation of the J-integral in the K-dominant region gives [29]:

$$J_K = \frac{K_I^2 + K_{II}^2}{\bar{E}} = \frac{|K|^2}{\bar{E}}\ . \tag{5}$$

Owing to the path-independency of the J-integral [29], J_K is equal to J_{loc} (Eq. (2)), so that

$$J_K = \mathcal{W}_o = \mathcal{W}_{n_o} + \mathcal{W}_{t_o}\ . \tag{6}$$

Irwin's virtual crack closure relation holds in LEFM: $\mathcal{G} = |K|^2/E$. So, a consistent connection between LEFM models and CZM models will be that $\mathcal{G} = \mathcal{W}_o$, if $\tilde{\xi}_o$ is small enough for LEFM assumptions to be valid.

2.2. Definitions of mode-mixedness

There are several definitions of mode-mixedness in the cohesive-zone literature (Fig. 2). The one we will focus on in this paper has a direct connection with the concept of a phase angle in LEFM. It is defined in terms of the ratio of the work done against each mode of deformation, so that, at any point along the interface, the local phase angle is

$$\psi(x_1) = \tan^{-1}\left(\sqrt{\frac{\mathcal{W}_t(x_1)}{\mathcal{W}_n(x_1)}}\right) \tag{7}$$

As x_1 approaches zero, this tends to the crack-tip phase angle, which is defined as [22,32]

$$\psi_o = \tan^{-1}\left[\sqrt{\frac{\mathcal{W}_{t_o}}{\mathcal{W}_{n_o}}}\right]\ . \tag{8}$$

The distance over which $\psi(x_1)$ is equal to ψ_o decreases with decreasing cohesive length, ξ_o [16,27,28].

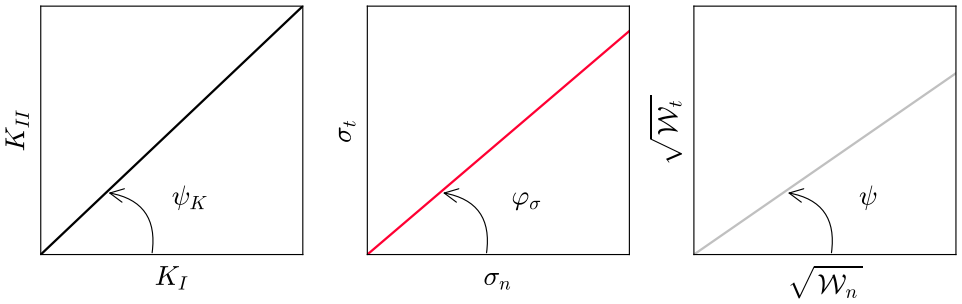

Fig. 2. Definition of (a) the phase angle ψ_K in LEFM; (b) the traction ratio, φ_σ; (c) the phase angle in a cohesive-zone model ψ.

For the special case of uncoupled cohesive laws, no modulus mismatch across the interface, and a very small value of $\tilde{\xi}_o$, the mode-I and mode-II work done against crack-tip tractions can be identified with K_I and K_{II} through Eq. (6) as[1]

$$\mathcal{W}_{n_o} = K_I^2/\bar{E}$$

$$\mathcal{W}_{t_o} = K_{II}^2/\bar{E} \quad . \tag{9}$$

The phase angle used in LEFM is defined as:

$$\psi_K = \tan^{-1}\left(\frac{K_{II}}{K_I}\right) \quad . \tag{10}$$

Therefore, as has been shown to be the case [16,27], ψ_o is expected to equal ψ_K under these conditions. Furthermore, if there is a modulus mismatch across the interface, ψ_o, scales with the elastic properties and cohesive length as predicted by LEFM [16,27,33].

It is noted that an alternative measure of mode-mixedness (Fig. 2), based on the ratio of the two tractions:

$$\varphi_\sigma(x_1) = \tan^{-1}\left[\frac{\sigma_t(x_1)}{\sigma_n(x_1)}\right] \tag{11}$$

can vary with the choice of cohesive law. It does not have the potential advantage of ψ_o, in linking crack-tip deformation to macroscopic conditions under LEFM conditions.

Under LEFM conditions, the magnitude of the stresses within the K field region are dictated by the stress-intensity factors. So, $\varphi_\sigma(x_1) = \psi_K$ in this region. However, it is axiomatic to LEFM that fracture is controlled by the deformation at the crack tip, and that the K-field controls this deformation through J_K. Therefore, it would seem to be an unnecessary restriction on modelling mixed-mode fracture to impose an additional constraint on cohesive laws that the crack-tip stresses in the entire cohesive zone should be in the same ratio as the stress-intensity factors [34]. In conclusion, one expects $\varphi_\sigma(x_1) = \psi_K$ in the K field, but expects φ_σ to depend on the choice of cohesive law at the crack tip. Conversely, one expects $\psi(x_1)$ to equal ψ_K close to the crack tip, but for there to be no connection between $\psi(x_1)$ and ψ_K in the K-field.

The observation that $\psi_o = \psi_K$ has already been shown to be valid if the cohesive laws are uncoupled [16,27]. However, a consideration of Eq. (2) for the case when the cohesive-laws are coupled indicates that the ratio between the two quantities ($\mathcal{W}_n$ and $\mathcal{W}_t$) may depend on the loading path, as discussed in Ref. [35]. In such a case there may not be a unique relationship between ψ_K and ψ_o. This could have implications for the use of LEFM to predict the failure of interfaces if the fracture-process mechanism behaves in accordance with a coupled traction–separation law. Mixed-mode LEFM models are all predicated on an assumption that deformation at the crack tip, where fracture takes place, is uniquely defined by K_I and K_{II}, with no path dependence. If coupled laws give path-dependent deformation at the crack tip, then it would imply that the use of LEFM may implicitly require the assumption of uncoupled cohesive laws. It is the purpose of this paper to explore this point.

In this context it should be emphasized that we are exploring the effects of using coupled and uncoupled laws, when $\tilde{\xi}_o$ is small enough for the problem to be in the LEFM limit. It has already been shown that, in this limit, uncoupled laws result in ψ_o being equal to ψ_k, provided sufficient care is taken to ensure that in finite element modelling the mesh size is small enough to observe the plateau in $\psi(x_1)$. We are interested in whether the same conclusion can be made for uncoupled laws, given the same care about mesh size and limitations on $\tilde{\xi}_o$.

This focus is in contrast to that of earlier work [27,32,36], which explored the crack-tip phase angle and mixed-mode fracture at large cohesive lengths, well away from the LEFM limit. This body of work indicates that, for large cohesive lengths, the crack-tip phase angle tends to move away from the values controlled by the local K-field to values controlled by the macroscopic loads and geometries, as suggested by Charalambides et al. [37]. For example, the paper by Conroy et al. [32] explores values of cohesive lengths that range from values slightly bigger than ones for which LEFM should unambiguously be valid to much larger values. At

[1] Occasionally, a form of this equation is used to define what are termed the mode-I and mode-II components of J_K or $\mathcal{G}$. However, this is not a rigorous perspective because J_K and $\mathcal{G}$ are scalar energy terms. They cannot be split into orthogonal components.

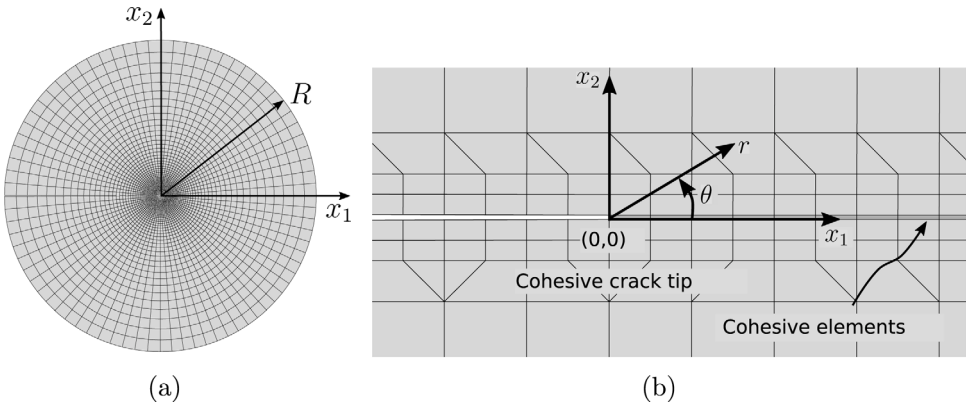

Fig. 3. The finite-element model used to describe the K-field domain; (a) shows the global model of the entire domain of radius R, (b) shows details of the elements at the crack tip.

the lower end, the phase angle for an uncoupled law approaches the LEFM value, while the phase angle for a coupled law shows a larger discrepancy. In this paper, we explore in detail the difference between coupled and uncoupled laws, while ensuring that we are unambiguously within the range where LEFM is valid.

3. Finite-element modelling

The problem was modelled by finite-element (FE) simulations, using the commercial code ABAQUS. The finite-element domain (of radius R) and the mesh for the mixed-mode K-field is shown in Fig. 3. A crack extends along the plane $x_2 = 0$, from $x_1 = -R$ to $x_1 = 0$. The traction–separation relationships used to model the cohesive zone were specified along the crack plane from $x_1 = 0$ to $x_1 = R$ (Fig. 3).

Quadratic plane-strain elements were used for the elastic solid, and quadratic cohesive elements of non-zero thickness were used in the cohesive zone. As can be seen from Fig. 3, a combination of quadrilateral and triangular elements allows for a structured increase in the size of the plane-strain elements as one moves away from the vicinity of the crack tip.

The mixed-mode cohesive laws were implemented as user-defined elements. The cohesive elements had a length[2] equal to $5 \times 10^{-7} R$ in the range $0 \leqslant x_1/R \leqslant 8.2 \times 10^{-3}$. The mesh was then gradually increased to $5 \times 10^{-2} R$ at $x_1/R = 1$. The height of the cohesive elements was equal to $5 \times 10^{-8} R$ along the cohesive interface. Only positive values of K_I were studied, so there was no issue with interpenetration.

Several potential-based mixed-mode cohesive laws were tested. Particular results are presented for the laws shown schematically in Fig. 4, and discussed in more detail in Appendix: an uncoupled trapezoidal law of [22], an uncoupled linear law [16,28], and the coupled Park–Paulino–Roesler (PPR) law [38,39].

3.1. Boundary conditions

The displacement components, u_1 and u_2, are related to the singular field of Fig. 3 by [40]:

$$\mu(u_2 + \mathrm{i}\, u_1) = \frac{|K|\sqrt{r}}{2\sqrt{2\pi}} \left\{ \frac{3-\bar{\nu}}{1+\bar{\nu}} \mathrm{i}\, \mathrm{e}^{-\mathrm{i}(\theta/2-\psi_K)} - \left[\mathrm{i}\, \mathrm{e}^{\mathrm{i}(\theta/2+\psi_K)} + \sin\theta\, \mathrm{e}^{-\mathrm{i}(\theta/2+\psi_K)} \right] \right\}, \tag{12}$$

where μ is the shear modulus, $\bar{\nu} = \nu$ in plane stress and $\bar{\nu} = \nu/(1-\nu)$ in plane strain, ν is Poisson's ratio, and the magnitude of the stress intensity factors is $|K| = \sqrt{K_I^2 + K_{II}^2}$. These displacement components are prescribed remotely on the boundary at $r = R$ by means of a user-defined ABAQUS subroutine. The magnitude of $|K|$ is varied through incremental changes in u_1 and u_2, such that ψ_K is kept at the desired value.

The application of displacements that match those expected in an LEFM field does not, by itself, ensure that a K-controlled stress field will be established. This requires an additional condition that both ξ_{n_o}/R and ξ_{t_o}/R are small enough. Although the geometry of Fig. 3 is the conventional one used to describe K-fields in infinite bodies with semi-infinite cracks, it must be remembered that R introduces an arbitrary length scale that will determine if the cohesive zone satisfies the small-scale conditions or not.

[2] This element size should be compared to the cohesive length, which is about $0.0015R$ for all the calculations. This satisfies the condition for mesh sensitivity [28].

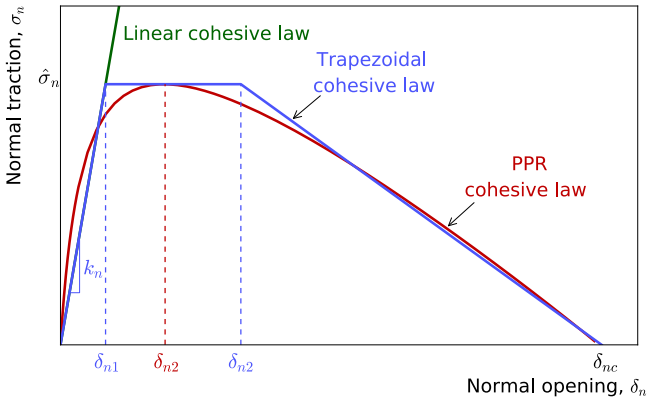

Fig. 4. Schematic illustration of the mode-I cohesive law for: a trapezoidal law, a linear law and the Park–Paulino–Roesler (PPR) with $\alpha = 1.98$. The shape of the PPR cohesive law depends on parameter α, which is defined in Appendix.

3.2. Measurement of mode-mixedness

The normal, $\sigma_n(x_1)$, and shear, $\sigma_t(x_1)$, tractions acting in the cohesive zone, and the corresponding normal, $\delta_n(x_1)$, and tangential, $\delta_t(x_1)$, openings were used to monitor the mode mixedness for all points along the cohesive zone ($x_1 \geq 0$, $x_2 = 0$). The work done against normal tractions, $\mathcal{W}_n$, was calculated for each point in the cohesive zone by integrating the area under the mode-I component of the traction–separation law for all increments up to the current level of δ_n, in accordance with Eq. (1). Similarly, $\mathcal{W}_t$ was determined from the area under the mode-II component of the traction–separation law up to the current level of δ_t. From these calculations of $\mathcal{W}_n$ and $\mathcal{W}_t$, the phase angle, $\psi(x_1)$, could be determined at every point ahead of the crack. The value of $\varphi_\sigma(x_1)$ was computed directly from the corresponding values of the tractions.

4. Results

The results presented in this section are divided into two main classes. In the first set of results, the loading is done in such a way that ψ_K remains constant throughout the loading procedure. This is described as proportional loading. In the second set of results, the loading is done in such a way that ψ_K changes during the loading procedure. This is described as non-proportional loading.

4.1. Proportional loading

4.1.1. Uncoupled cohesive laws

Fig. 5 shows the normal and shear tractions ahead of the crack tip for an uncoupled, linear cohesive law (Appendix A.1) for a fixed value of the phase angle, ψ_K=45°, and for three different values of ξ_t/ξ_n (Note that for a linear law $\xi_{to} = \xi_t$ and $\xi_{no} = \xi_n$). The value of $\tilde{\xi}_{no}/R$ for this plot is equal to 0.01375, which satisfies small-scale conditions. The excellent agreement between the numerical results and the asymptotic K field can be seen from this plot for both the opening and shear tractions. The K field under these conditions extends to within about $0.01R$ from the crack tip, with the relationship between the cohesive length and the extent of the singular field being visible from Fig. 5(b).

Fig. 5 provides what might be considered to be a classic understanding of LEFM: an inverse square root relationship between stress and distance from the crack tip, with a magnitude given by K_I and K_{II}, but which breaks down near the crack tip.[3] This verifies the ability of a cohesive-zone model to describe LEFM under appropriate small-scale conditions.

The variation of the phase angle, $\psi(x_1)$, with x_1, is illustrated in Fig. 6 with the same three cohesive laws (with different ξ_t/ξ_n ratios) as the plots in Fig. 5, but with three different phase angles. As expected, ψ_o tends to ψ_K close to the crack tip in all cases, but generally deviates from this equality in the K field. The exception is the special case of $\xi_t/\xi_n = 1$, for which $\psi(x_1)$ equals ψ_K for all values of x_1/R. This is because the ratio of the two stresses is equal to the square root of the ratio of the two modes of work in this law. Therefore, there is a special case agreement between $\psi(x_1)$ and ψ_K within the K field where the stresses must also scale with ψ_K. For the other cohesive laws, the same agreement between the stresses and ψ_K applies, but now the ratio of the stresses is not the same as the ratio of the square root of the work.

This point is emphasized in Fig. 7, which shows how the traction ratios, represented by the phase angle φ_σ, vary with x_1. For $\xi_n/\xi_t = 1$, the traction ratio is identical to the square root of the work ratios for a linear cohesive law. Therefore, $\psi_\sigma = \psi_K$, both near the crack tip and in the K field. For other values of ξ_n/ξ_t, $\varphi_\sigma = \psi_K$ only in the K field. However, it should be remembered that it is at the crack tip where fracture occurs, and where one needs a measure of mode-mixedness that can be linked to LEFM. As discussed earlier, such a measure is provided by ψ_o, which equals ψ_K for an uncoupled law.

[3] It should be noted that, for this law, the asymptotic stresses near the crack tip are limited by the requirement for a finite work at the crack tip, rather than any intrinsic value of cohesive strength.

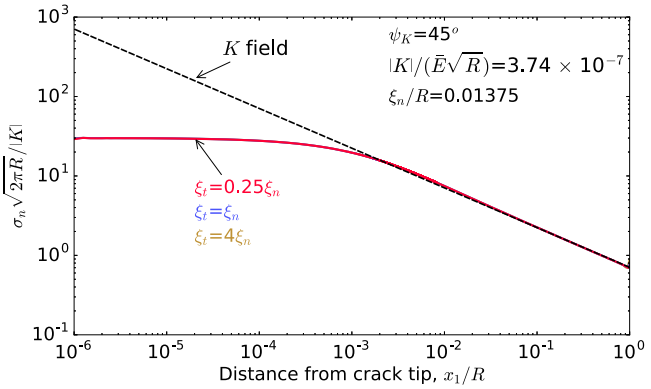

(a) Normal tractions

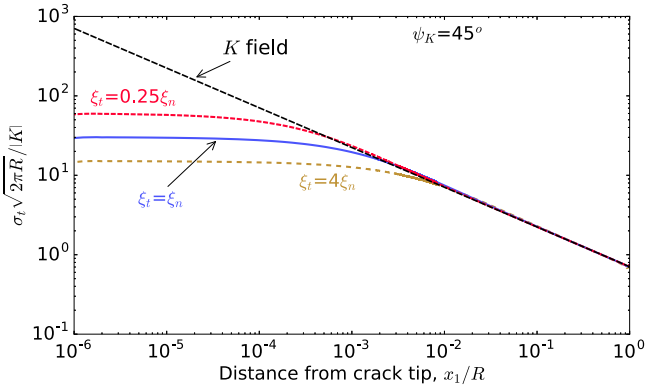

(b) Shear tractions

Fig. 5. (a) The normal tractions and (b) the shear tractions along x_1 for uncoupled, linear cohesive laws at fixed values of ξ_n/R and $|K|/\bar{E}\sqrt{R}$, and at three different values of ξ_{t_o}/ξ_{n_o}. The phase angle, ψ_K is equal to 45°.

Similar conclusions can be drawn from calculations conducted using uncoupled laws with different shapes. Although this has been demonstrated before for beam-like geometries [16], here we show the results for a K-field geometry using a trapezoidal law (described in Appendix A.1) for two values of mode-mixedness. Fig. 8 shows how the stress field evolves near the crack tip for $\psi_K = 45^o$, and a peak traction ratio $\hat{\sigma}_t/\hat{\sigma}_n = 2$. The length of the fracture process zone is less than 1% R and, in the K-field zone ($x_1/R > 10^{-2}$), the normal and shear tractions are identical to the asymptotic field. In this case, the tractions of the uncoupled cohesive law are at their maximum values, established by their cohesive strengths, all the way to the cohesive crack tip, because neither law has entered the softening regime under the conditions for which the plot has been made. It should be emphasized that ξ_o is small enough for LEFM to be valid, as can be seen from the stress field of Fig. 8.

Fig. 9 shows how the phase angle $\psi(x_1)$ varies with x_1 for $\psi_K = 45^o$ and 60^o. As before, it can be seen that the crack-tip phase angle, ψ_o tends to ψ_K. Away from the crack-tip region, there is no particular significance to this partition of work. However, it should be noted that, for these calculations, much of the K-field is associated with the initial, linear portion of the traction–separation law. This means that, for the two cases with identical mode-I and mode-II cohesive laws, the laws look like linear laws with equal cohesive lengths. As discussed in connection with Fig. 6, this means that in the K-field region the special case of $\psi(x_1) = \psi_K$ is met.

4.1.2. Coupled cohesive laws

The results for the coupled cohesive law developed by Park et al. [38], which we refer to as the PPR law, are described in this section.

Fig. 10 shows the normal and shear tractions ahead of the crack tip with $\psi_K = 45^o$, and with values of K and cohesive strengths corresponding to those used for Fig. 8. In this case, the cohesive-zone is fully developed, so the stresses at the crack tip are approximately zero. As with the uncoupled law, the cohesive-length scale, ξ_o, is so small that the stresses are described by the asymptotic K-field at distances greater than about $0.01R$ from the crack tip. Again, this confirms the ability of a cohesive-zone model to describe LEFM under appropriate conditions.

The phase angle, ψ, is plotted in Fig. 11 for three peak-traction ratios, $\hat{\sigma}_t/\hat{\sigma}_n$, and two values of ψ_K. These plots illustrate the effect of different parameters for the PPR cohesive law. A key difference between the results for this form of a coupled law, and the

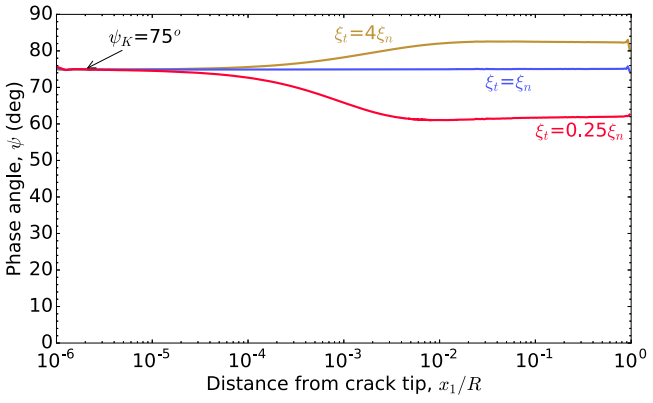

(a)

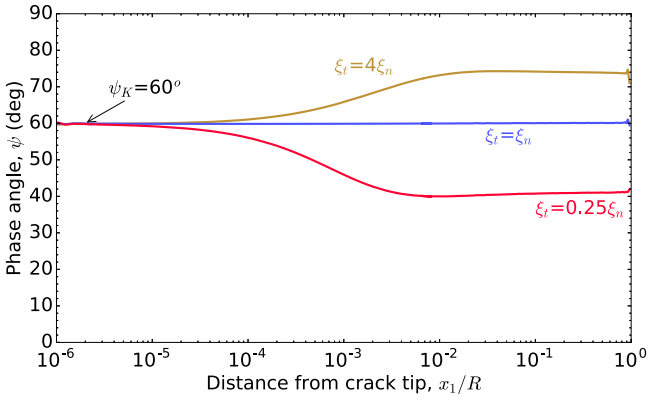

(b)

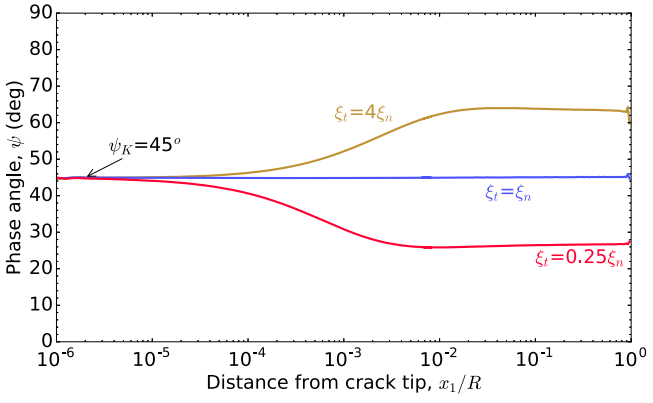

(c)

Fig. 6. The variation of the phase angle with distance ahead of the crack tip for three uncoupled linear cohesive laws, with $\xi_t/\xi_n = 4$, 1 and 0.25: (a) $\psi_K = 75°$, (b) $\psi_K = 60°$, and (c) $\psi_K = 45°$. For these plots, $|K|/\bar{E}\sqrt{R} = 3.74 \times 10^{-7}$, and $\xi_n/R = 0.01375$.

results for uncoupled cohesive laws, is that, in general, $\psi_o \neq \psi_K$. The only situation in which $\psi_o = \psi_K$ is the special case of ψ_K=45^o, when the shear and normal laws are identical. A similar result that, in general, $\psi_o \neq \psi_K$ for coupled mixed-mode laws was found when several other coupled cohesive laws were explored, including those of Xu and Needleman [18], and Sørensen and Goutianos [41].

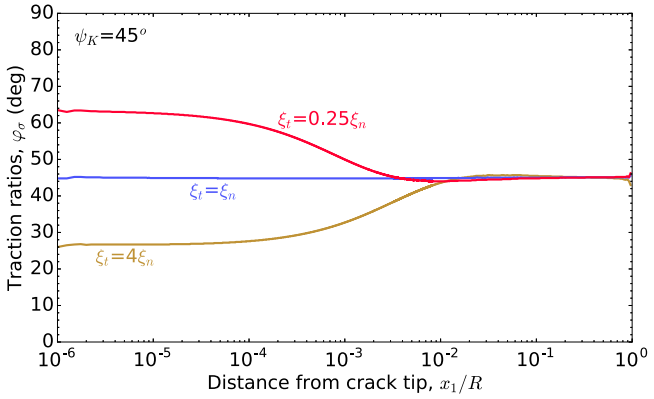

Fig. 7. The variation of φ_σ for the three uncoupled linear cohesive laws of Fig. 5. ψ_K =45 ° and three different ratios ξ_t/ξ_n.

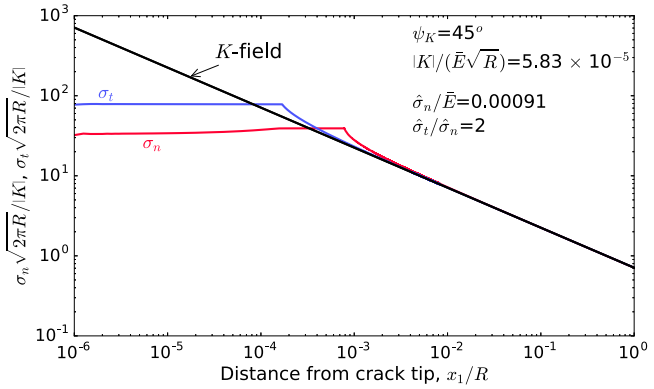

Fig. 8. Normal and shear tractions along axis x_1 for an uncoupled trapezoidal cohesive law. The non-dimensional parameters for this plot are given in Table A.1 for $\hat{\sigma}_t/\hat{\sigma}_n = 2$.

The reason for the discrepancy between ψ_K and ψ_o can be seen by a simple examination of the form of the equations. If, in general, $\sigma_n = f_n(\delta_n, \delta_t)$ and $\sigma_t = f_t(\delta_n, \delta_t)$, then the crack-tip phase angle, which from Eq. (2) is given by

$$\psi_o = \tan^{-1}\left(\frac{\int_0^{\delta_{t_o}} f_t(\delta_n', \delta_t')d\delta_t'}{\int_0^{\delta_{n_o}} f_n(\delta_n', \delta_t')d\delta_n'}\right)^{1/2}, \tag{13}$$

will generally depend on how δ_t varies with δ_n, and it is going to be path dependent. In particular, there is no reason why ψ_o should be related to ψ_K.

4.2. Non-proportional loading

In the previous section, we showed that $\psi_o = \psi_K$ for uncoupled laws and proportional loading; but this identity was valid only for very special forms of coupled laws. In this section, we explore the effect of non-proportional loading on this relationship. Specifically, we do this by determining the evolution of the phase angle as the geometry is loaded to the same final conditions ($\psi_k = 45^o$), but following two different loading paths, p_1 and p_2, illustrated schematically in Fig. 12.

Fig. 13 shows how the phase angle $\psi(x_1)$ varies with x_1 for an uncoupled trapezoidal law at four discrete points along the two non-proportional loading paths, p_1 and p_2 identified in Fig. 12. It can be seen that the crack-tip phase angle, ψ_o, always matches the applied value of ψ_K, at all points during loading. Similar results were obtained for all the other paths and cohesive parameters that were explored.

The corresponding results for the PPR cohesive law are shown in Fig. 14. In this case, it will be remembered that ψ_o was not equal to ψ_K for proportional loading. Here the two parameters are in closer agreement for a trajectory that starts off dominated by mode-I. However, the two are even more divergent for the mode-II dominated trajectory than for the proportional trajectory, indicating clear evidence of path-dependence for the crack-tip phase angle. This path dependence of ψ_o was confirmed as being

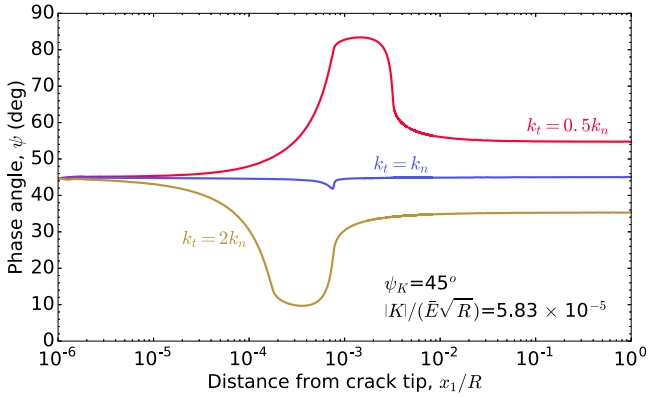

(a)

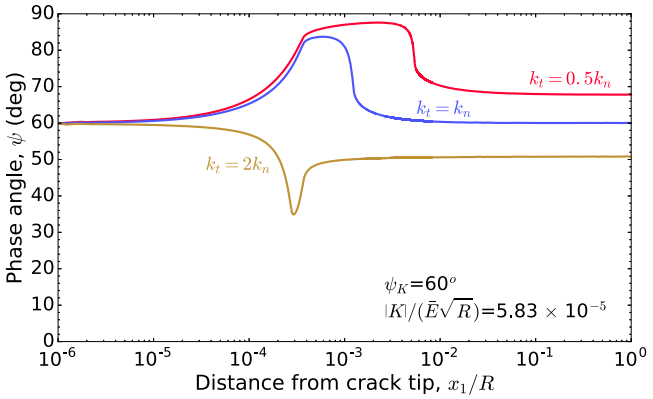

(b)

Fig. 9. Phase angle $\psi(x_1)$ along axis x_1 for uncoupled trapezoidal cohesive laws with varying stiffnesses and peak traction ratios: (a) ψ_K =45°, and (b) ψ_K =60°. The non-dimensional parameters for this plot are given in Table A.1 for the three values of k_t/k_n *e.g.* $\hat{\sigma}_t = 0.5\hat{\sigma}_n$ for $k_t = 0.5k_n$, $\hat{\sigma}_t = \hat{\sigma}_n$ for $k_t = k_n$ and $\hat{\sigma}_t = 2\hat{\sigma}_n$ for $k_t = 2k_n$. See Appendix A.1 for definitions of k_n and k_t.

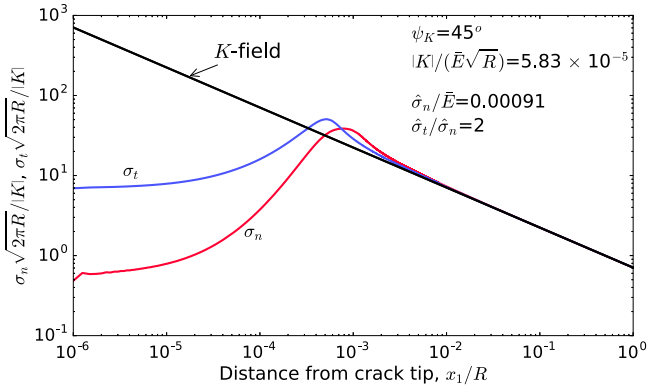

Fig. 10. Normal and shear tractions along axis x_1 when the fracture process zone is fully developed for the coupled PPR cohesive law. The non-dimensional parameters for this plot are given in Table A.2 for $\hat{\sigma}_t/\hat{\sigma}_n = 2$.

a general result for other paths and cohesive parameters for coupled laws. It should be emphasized that, in all cases, the total work at the crack tip remained the same. There was no path dependence to this quantity, as expected for potential-based laws. The path-dependency was only related to how the crack-tip work was partitioned between the two modes.

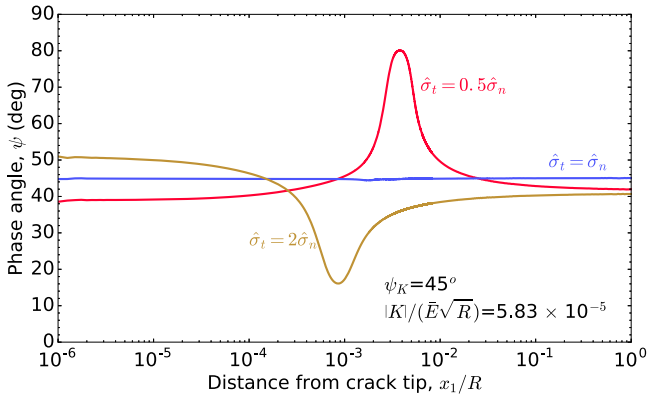

(a)

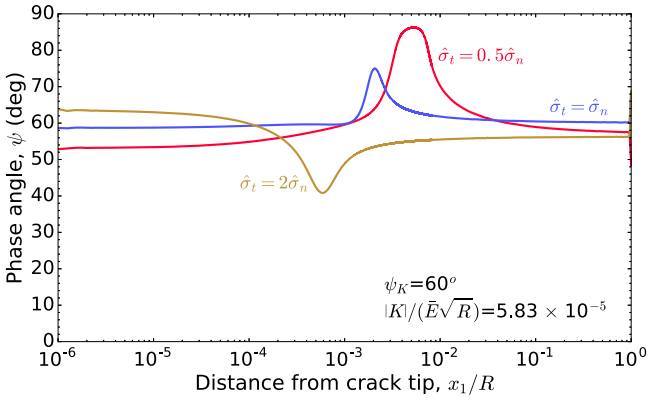

(b)

Fig. 11. Phase angle ψ along axis x_1 for coupled PPR cohesive laws with varying stiffnesses and peak traction ratios: (a) ψ_K =45°, and (b) ψ_K =60°. The non-dimensional parameters for this plot are given in Table A.2 for the three values of $\hat{\sigma}_t/\hat{\sigma}_n$.

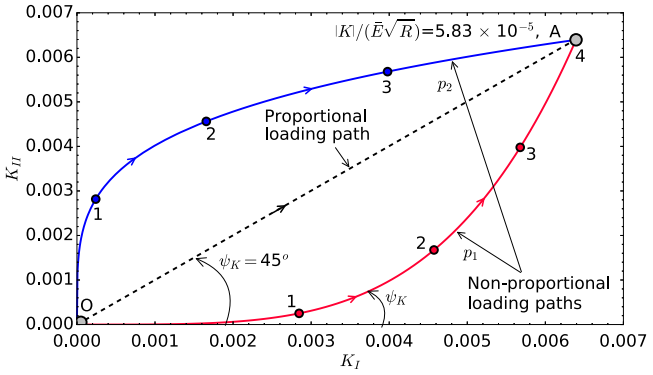

Fig. 12. Proportional-loading path OA (dashed line) and non-proportional-loading paths p_1 and p_2 (solid lines).

5. Discussion

5.1. LEFM assumptions

Mixed-mode loading in an LEFM framework is completely described by the energy-release rate, $\mathcal{G}$, and the phase angle, ψ_K. It is assumed that any small-scale deformation at the crack tip is uniquely described by these two parameters, which are both independent of the loading history. Therefore, in corresponding cohesive zone modelling, both the magnitude of the work done at the crack tip

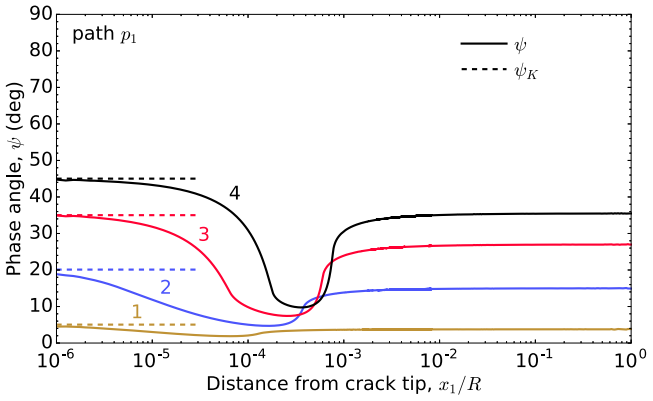

(a) points $1 \rightarrow 4$ along path p_1

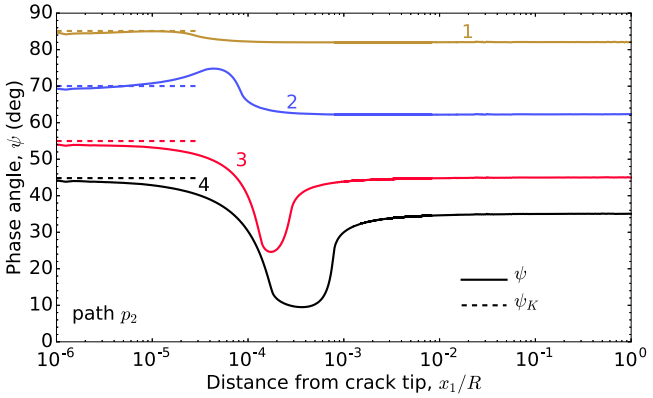

(b) points $1 \rightarrow 4$ along path p_2

Fig. 13. The variation of ψ with x_1 with an uncoupled trapezoidal law for four steps in a non-proportional loading process, as ψ_K increases along the non-proportional loading paths (a) p_1 and (b) p_2 shown in Fig. 12. The uncoupled cohesive law parameters are defined in Table A.1, with $\hat{\sigma}_t = 2\hat{\sigma}_n$.

during this deformation and the partition of this work into normal and shear components can be deduced uniquely from the two parameters.[4] Mixed-mode failure criteria used in LEFM analyses are all predicated on this concept of path-independence.

The use of potential-based traction–separation laws within a cohesive-zone framework, ensures the same total work is done against crack-tip tractions for any loading path under mixed-mode loading. Therefore, this class of cohesive law results in an agreement with one LEFM assumption: the energy-release rate does not depend on the loading history. However, not all potential-based cohesive laws match the second assumption: the LEFM partition of the work at the crack tip can be described only in terms of K_I and K_{II}.

The present paper confirms the earlier results of [16,27,28] that the LEFM assumption about the prediction of work is satisfied for uncoupled cohesive laws if $\tilde{\beta} \neq 0$.[5] However, it is shown here that coupled cohesive laws generally result in a different partition of crack-tip work from that assumed by LEFM. Furthermore, while the total work is path independent, this partition of crack-tip work can be path dependent. This conclusion has been illustrated by the results presented in this paper, but it was also confirmed by testing other potential-based coupled cohesive laws from the literature [18,38,41], with proportional and non-proportional loading paths.

5.2. Implications for LEFM mixed-mode failure criteria

The implicit assumption behind LEFM mixed-mode failure criteria is that an interface separates when the energy-release rate, $\mathcal{G}$, exceeds a critical value, Γ, which is identified as the toughness, and is a function of the phase angle: $\mathcal{G} \geq \Gamma(\psi_K)$. This functional

[4] This is rigorously correct only when the second Dundurs parameter, $\tilde{\beta}$, is equal to zero. When $\tilde{\beta} \neq 0$, LEFM cannot be used to partition the work done in deforming the crack-tip region into shear and normal components, although the total work is still given by the energy-release rate [33,42].

[5] LEFM requires an additional length parameter to represent the behaviour of uncoupled potential-based cohesive laws when $\tilde{\beta} \neq 0$ [16,27].

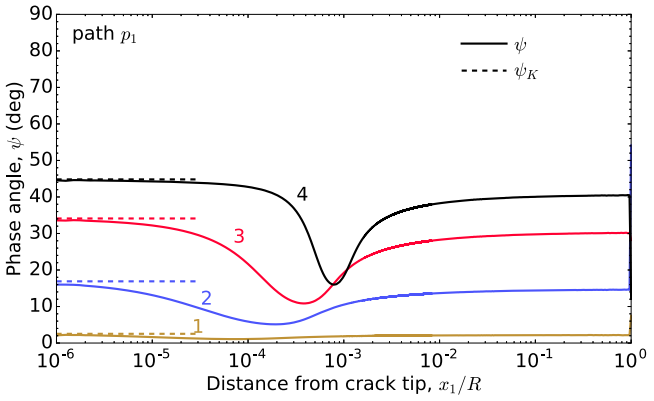

(a) points $1 \rightarrow 4$ along path p_1

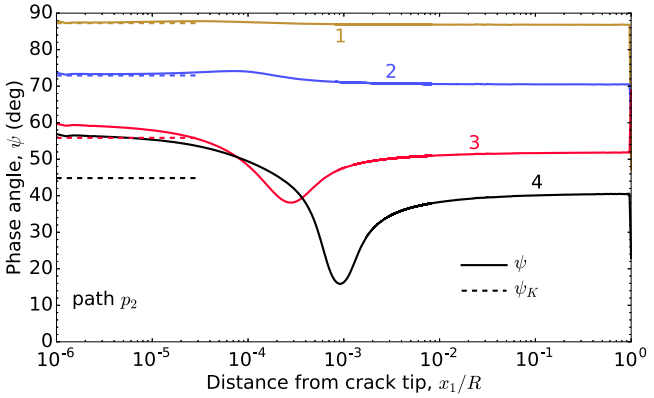

(b) points $1 \rightarrow 4$ along path p_2

Fig. 14. The variation of $\psi(x_1)$ with x_1 with a coupled PPR law for four steps in a non-proportional loading process, as ψ_K increases along the non-proportional loading paths (a) p_1 and (b) p_2 shown in Fig. 12. The uncoupled cohesive law parameters are defined in Table A.1, with $\hat{\sigma}_t = 2\hat{\sigma}_n$.

dependence of toughness on phase angle can take any form, including non-monotonic forms. However, in LEFM, the phase angle is defined only in terms of the geometry and the loads, and is path independent. Therefore, the toughness of an interface is implicitly assumed to be path independent.

In practice, most LEFM mixed-mode fracture tests are conducted under proportional loading, so that ψ_K is constant throughout a test. An envelope of toughness is developed as a function of ψ_K through a series of separate tests, each one exploring a different value of ψ_K. With this approach, it would not matter if the actual crack-tip phase angle, ψ_o, of the fracture process was incorrectly described by ψ_K, a unique mixed-mode failure envelope would always be developed that described the experimental results. This failure envelope could then be used predictively in design, under the same assumptions of LEFM and proportional loading.

It would be relatively easy to develop a cohesive-law that describes such limited data. Both coupled and uncoupled laws could work; indeed, even a law not based on a potential function could work, if the issue of path dependence is not explored. However, only the uncoupled law would be consistent with LEFM assumptions. More detailed experimental studies might reveal path-dependence, violating LEFM, in which case coupled laws derived from a potential function or cohesive laws not derived from a potential function might be more appropriate.

6. Conclusions

Different types of mixed-mode, potential-based cohesive laws under small-scale conditions have been used to explore how the behaviour of the crack-tip region compares to the assumptions that underpin linear-elastic fracture mechanics (LEFM). It has been shown that the fundamental assumptions of LEFM are fully consistent with uncoupled, potential-based laws. For these types of law, not only is the work done against crack-tip tractions independent of the loading path and equal to the value of the J-integral, but the partition of this work into the two orthogonal modes is also in agreement with LEFM assumptions. The crack-tip phase angle is equal to the phase angle of the surrounding K-field if small-scale conditions are met.

Coupled, potential-based cohesive laws result in the work done against the crack-tip tractions being path-independent and equal to that given by the J-integral (consistent with LEFM). However, the partition of this work into normal and shear components does not necessarily agree with that indicated by the surrounding K-field, even under small-scale conditions. In particular, the crack-tip phase angle can be path dependent.

These results have implications for the interpretation of mixed-mode fracture experiments and design based on LEFM concepts. LEFM assumes that deformation at a crack tip is uniquely described by the K-field. It also assumes that the local conditions for mixed-mode crack advance are controlled by K_I and K_{II}, and, hence, mixed-mode failure is independent of the loading path. However, if the normal and shear deformation processes at the crack tip are coupled, these assumptions would generally be violated to some degree.

A full understanding of mixed-mode failure criteria requires path dependence to be explored. In the absence of any significant path dependence being observed experimentally, uncoupled, potential-based cohesive laws with suitable empirical mixed-mode failure criteria would seem to be adequate, and, perhaps, the easiest to implement numerically. In addition, the use of path-dependent functions or coupled laws would need to be validated to ensure they did not introduce stronger path-dependence than merited by the experimental results. Only if significant path dependence that needs to be modelled is observed experimentally, would it seem to be imperative to use a coupled law, or path-dependent cohesive laws.

Declaration of competing interest

The authors declare that they have no known competing financial interests or personal relationships that could have appeared to influence the work reported in this paper.

Appendix. Potential-based mixed-mode cohesive laws

A.1. Uncoupled cohesive laws

Two forms of mixed-mode uncoupled cohesive laws are used in this study. The first is a special case of linear laws, for which the tractions are linearly dependent on the displacements until failure. Mathematically, these are described by

$$\sigma_n(\delta_n) = k_n\delta_n \tag{A.1}$$

$$\sigma_t(\delta_t) = k_t\delta_t\ , \tag{A.2}$$

where k_n and k_t are the stiffnesses of the two modes, which need not be identical. The peak tractions were set high enough that fracture did not occur in this study. However, they can easily be added if fracture needs to be modelled explicitly. It should be noted that a physical manifestation of a linear-elastic cohesive law could be an interface bonded by compliant brittle elastic springs. However, from a modelling perspective, linear laws have the unique feature that the instantaneous cohesive-lengths [28],

$$\xi_n = 2\bar{E}/k_n \ \text{ and } \ \xi_t = 2\bar{E}/k_t\ , \tag{A.3}$$

do not vary during loading. Furthermore, the simplicity of linear cohesive-laws means that the results of all calculations performed with them can be expressed in terms of only four non-dimensional parameters:

$$\frac{\xi_n}{R},\ \frac{\xi_t}{\xi_n},\ \frac{|K|}{\bar{E}\sqrt{R}},\ \psi_K\ ,$$

where the first two terms describe the cohesive laws, and the second two terms describe the remote loading.

For completeness, Eqs. (A.1) and (A.2), can be used to show that the potential function is

$$\Phi = \frac{k_n\delta_n^2}{2} + \frac{k_t\delta_t^2}{2}\ . \tag{A.4}$$

Since

$$\frac{\partial\sigma_n(\delta_n)}{\partial\delta_t} = \frac{\partial\sigma_t(\delta_t)}{\partial\delta_n} = 0 \tag{A.5}$$

and therefore the mixed mode linear uncoupled laws are based on a potential function.

The second form of uncoupled law used in this study are trapezoidal laws [22]. The tractions for these laws increase linearly with displacement until the normal and tangential displacements are δ_{n_1} and δ_{t_1}; at which point the peak tractions are $\hat{\sigma}_n$ and $\hat{\sigma}_t$, respectively. The tractions remain at these levels while the relevant displacements remain less than δ_{n_2} and δ_{t_2}, at which point they drop linearly to zero at $\delta_n = \delta_{n_c}$ and $\delta_t = \delta_{t_c}$. These laws can be expressed in the range $-90^o \le \varphi_\delta \le 90^o$ as

$$\sigma_n = \hat{\sigma}_n\left[\frac{\delta_n}{\delta_{n_1}} - \frac{\left\langle\delta_n-\delta_{n_1}\right\rangle^1}{\delta_{n_1}} - \frac{\left\langle\delta_n-\delta_{n_2}\right\rangle^1}{\left(\delta_{n_c}-\delta_{n_2}\right)} + \frac{\left\langle\delta_n-\delta_{n_c}\right\rangle^1}{\left(\delta_{n_c}-\delta_{n_2}\right)}\right]$$

Table A.1
Parameters for the uncoupled trapezoidal cohesive law used in the calculations for this paper. The critical mode-I and mode-II instantaneous cohesive lengths are defined as $\xi_n^c = \bar{E}\delta_{n_c}^2/\Gamma_n$ and $\xi_t^c = \bar{E}\delta_{t_c}^2/\Gamma_t$.

$\hat{\sigma}_n/\bar{E}$		0.001	
ξ_n^c/R		0.0115	
$\delta_{n_1}/\delta_{n_c}$		0.01	
$\delta_{n_1}/\delta_{n_2}$		0.05	
σ_t/σ_n	0.5	1	2
k_t/k_n	0.5	1	2
$\delta_{t_1}/\delta_{t_c}$	0.0046	0.01	0.025
$\delta_{t_1}/\delta_{t_2}$	0.05	0.05	0.05

$$\sigma_t = \hat{\sigma}_t \left[\frac{\delta_t}{\delta_{t_1}} - \frac{\left\langle \delta_t - \delta_{t_1} \right\rangle^1}{\delta_{t_1}} - \frac{\left\langle \delta_t - \delta_{t_2} \right\rangle^1}{\left(\delta_{t_c} - \delta_{t_2}\right)} + \frac{\left\langle \delta_t - \delta_{t_c} \right\rangle^1}{\left(\delta_{t_c} - \delta_{t_2}\right)} \right] \tag{A.6}$$

where $\langle \cdots \rangle$ are Macaulay brackets [43]. Macaulay brackets of the form $\langle \delta - \delta_i \rangle^1$ are interpreted as being equal to 0 when $\delta < \delta_i$, or equal to $(\delta - \delta_i)$ when $\delta \geq \delta_i$.

The non-dimensional presentation of results for these trapezoidal laws is slightly more complicated than for the linear laws, because of the additional parameters required to describe the laws. The problem is completely described by ten non-dimensional groups. There are the two loading parameters, $|K|/(\bar{E}\sqrt{R})$ and ψ_K, and eight parameters that describe the cohesive laws. The values of these eight parameters that are used in this paper are given in Table A.1.

Finally, it should be noted that what are termed as "uncoupled" mixed-mode cohesive laws are actually coupled through a failure criterion of the general form

$$f\left(\frac{\mathcal{W}_n}{\Gamma_I}, \frac{\mathcal{W}_t}{\Gamma_{II}}\right) = 1, \tag{A.7}$$

where Γ_I and Γ_{II} are the areas under the mode-I and mode-II cohesive laws. When this condition is met, both sets of tractions are set to zero. Although, it is not the point of this study to explore fracture, and the important results of this paper can be obtained at arbitrary points during loading, it can be shown that Eq. (A.7) can be expressed as a failure criterion of the form $\Gamma = \Gamma(\psi_K)$ used in LEFM. Under general mixed-mode loading, $\Gamma(\psi_K) = W_n^* + W_t^*$, where W_n^* and W_t^* at failure are given by

$$W_n^* = \frac{\Gamma(\psi_K)}{1 + \tan^2 \psi_K} \text{ and } W_t^* = \frac{\Gamma(\psi_K)\tan^2(\psi_K)}{1 + \tan^2 \psi_K} \tag{A.8}$$

If for example, a simple failure criterion is used such as

$$\frac{W_n^*}{\Gamma_I} + \frac{W_t^*}{\Gamma_{II}} = 1, \tag{A.9}$$

then the failure criterion of Eq. (A.7) can be written as

$$\Gamma(\psi_K) = \Gamma_I \frac{1 + \tan^2 \psi_K}{1 + (\Gamma_{II}/\Gamma_I)\tan^2 \psi_K} \tag{A.10}$$

An alternative way to demonstrate that "uncoupled" laws are actually coupled is to re-write Eq. (A.7) using the mode-I and mode-II peak tractions. Assuming linear laws (Eqs. (A.1) and (A.2)):

$$\Gamma_I = \frac{\hat{\sigma}_n^2}{2k_n} \text{ and } \Gamma_{II} = \frac{\hat{\sigma}_t^2}{2k_t} \tag{A.11}$$

and

$$W_n = \Gamma_I \left(\frac{\sigma_n}{\hat{\sigma}_n}\right)^2 \text{ and } W_t = \Gamma_{II} \left(\frac{\sigma_t}{\hat{\sigma}_t}\right)^2. \tag{A.12}$$

Then, the failure criterion of Eq. (A.9) is given by

$$\left(\frac{\sigma_n^*}{\hat{\sigma}_n}\right)^2 + \left(\frac{\sigma_t^*}{\hat{\sigma}_t}\right)^2 = 1 \tag{A.13}$$

where the tractions at failure, as a function of ψ_K are

$$\sigma_n^* = \hat{\sigma}_n \sqrt{\frac{1}{(\Gamma_I/\Gamma_{II})\tan^2 \psi_K + 1}} \tag{A.14}$$

Table A.2
Parameters for the coupled PPR cohesive law used in the calculations for this paper. The critical mode-I and mode-II instantaneous cohesive lengths are defined as $\xi_n^c = \bar{E}\delta_{n_c}^2/\Gamma_n$ and $\xi_t^c = \bar{E}\delta_{t_c}^2/\Gamma_t$.

$\hat{\sigma}_n/\bar{E}$		0.00091	
ξ_n^c/R		0.0115	
α		1.9	
$\delta_{n_1}/\delta_{n_c}$		0.1	
$\hat{\sigma}_t/\hat{\sigma}_n$	0.5	1	2
ξ_t^c/R	0.0539	0.0115	0.0018
β	1.95	1.9	1.6
$\delta_{t_1}/\delta_{t_c}$	0.04	0.1	0.23

and

$$\sigma_t^* = \hat{\sigma}_t \sqrt{\frac{(\Gamma_I/\Gamma_{II})\tan^2\psi_K}{(\Gamma_I/\Gamma_{II})\tan^2\psi_K + 1}} \tag{A.15}$$

A.2. Park–Paulino–Roesler (PPR) cohesive law

A number of different path-independent, coupled mixed-mode cohesive laws are available in the literature. In the present study, the Park–Paulino–Roesler (PPR) cohesive law is used [38,39]. The normal and shear tractions are given by:

$$\sigma_n(\delta_n,\delta_t) = \frac{\Phi_I}{\delta_{n_c}}\left[m\left(1-\frac{\delta_n}{\delta_{n_c}}\right)^{\alpha}\left(\frac{m}{\alpha}+\frac{\delta_n}{\delta_{n_c}}\right)^{(m-1)} - \alpha\left(1-\frac{\delta_n}{\delta_{n_c}}\right)^{\alpha-1}\left(\frac{m}{\alpha}+\frac{\delta_n}{\delta_{n_c}}\right)^{m}\right]$$
$$\left[\Phi_{II}\left(1-\frac{|\delta_t|}{\delta_{t_c}}\right)^{\beta}\left(\frac{n}{\beta}+\frac{|\delta_t|}{\delta_{t_c}}\right)^{n} + \langle\Gamma_t-\Gamma_n\rangle^1\right]$$

$$\sigma_t(\delta_n,\delta_t) = \frac{\Phi_{II}}{\delta_{t_c}}\left[n\left(1-\frac{|\delta_t|}{\delta_{t_c}}\right)^{\beta}\left(\frac{n}{\beta}+\frac{|\delta_t|}{\delta_{t_c}}\right)^{(n-1)} - \beta\left(1-\frac{|\delta_t|}{\delta_{t_c}}\right)^{\beta-1}\left(\frac{n}{\beta}+\frac{|\delta_t|}{\delta_{t_c}}\right)^{n}\right]$$
$$\left[\Phi_I\left(1-\frac{\delta_n}{\delta_{n_c}}\right)^{\alpha}\left(\frac{m}{\alpha}+\frac{\delta_n}{\delta_{n_c}}\right)^{m} + \langle\Gamma_n-\Gamma_t\rangle^1\right]\frac{\delta_t}{|\delta_t|} \tag{A.16}$$

where α and β are non-dimensionless constants, δ_{n_c} and δ_{t_c} are the mode-I and mode-II critical openings when the tractions become zero, and Γ_n and Γ_t are the toughness values for mode-I and mode-II. The energy constants Φ_n and Φ_t are given by:

$$\Phi_n = \left(-\Gamma_n\right)^{\langle\Gamma_n-\Gamma_t\rangle^1/(\Gamma_n-\Gamma_t)}\left(\frac{\alpha}{m}\right)^{m}$$
$$\Phi_t = \left(-\Gamma_t\right)^{\langle\Gamma_t-\Gamma_n\rangle^1/(\Gamma_t-\Gamma_n)}\left(\frac{\beta}{n}\right)^{n}. \tag{A.17}$$

The non-dimensional exponents m and n are given by:

$$m = \frac{\alpha(\alpha-1)(\delta_{n_1}/\delta_{n_c})^2}{(1-\alpha\delta_{n_1}/\delta_{n_c})}, \quad n = \frac{\beta(\beta-1)(\delta_{t_1}/\delta_{t_c})^2}{(1-\beta\delta_{t_1}/\delta_{t_c})}. \tag{A.18}$$

where δ_{n_1} and δ_{t_1} are the normal and tangential openings corresponding to the pure mode-I and pure mode-II peak tractions, respectively.

The problem of this paper is completely described by ten non-dimensional groups, including the two loading parameters, $|K|/(\bar{E}\sqrt{R})$ and ψ_K. The eight parameters used in this paper that describe the cohesive laws are given in Table A.2. The parameters are chosen in such a way so as to ensure that the shape of pure mode-I and mode-II cohesive laws are similar to the shape of the corresponding mode-I and mode-II uncoupled cohesive laws. They have identical peak tractions, critical openings and fracture energies as the corresponding uncoupled laws (Table A.1).

References

[1] Hillerborg A, Modéer M, Petersson P-E. Analysis of crack formation and crack growth in concrete by means of fracture mechanics and finite elements. Cem Concr Res 1976;6:773–81.
[2] Needleman A. A continuum model for void nucleation by inclusion debonding. J Appl Mech Trans ASME 1987;54:525–31.

[3] Marshall DB, Cox BN, Evans AG. The mechanics of matrix cracking in brittle-matrix fiber composites. Acta Metall 1985;33:2013–21.
[4] Tvergaard V, Hutchinson JW. The relation between crack growth resistance and fracture process parameters in elastic-plastic solids. J Mech Phys Solids 1992;40:1377–97.
[5] Reinoso J, Paggi M, Blàzquez A. A nonlinear finite thickness cohesive interface element for modeling delamination in fibre-reinforced composite laminates. Composites B 2017;15:116–28.
[6] Yang QD, Thouless MD, Ward SM. Numerical simulations of adhesively-bonded beams failing with extensive plastic deformation. J Mech Phys Solids 1999;47:1337–53.
[7] Mohammed I, Liechti KM. Cohesive zone modeling of crack nucleation at bimaterial corners. J Mech Phys Solids 2000;48:735–64.
[8] Sørensen BF, Goutianos S, Jacobsen TK. Strength scaling of adhesive joints in polymer-matrix composites. Int J Solids Struct 2009;46:741–61.
[9] Overgaard LCT, Lund E. Structural collapse of a wind turbine blade. Part b: Progressive interlaminar failure models. Composites A 2010;41:271–83.
[10] Dugdale DS. Yielding of steel sheets containing slits. J Mech Phys Solids 1960;8:100–4.
[11] Barenblatt GI. The mathematical theory of equilibrium cracks in brittle fracture. Adv Appl Mech 1962;7:55–129.
[12] Inglis CE. Stresses in a plate due to the presence of cracks and sharp corners. Trans Inst Nav Archit 1913;55:219–30.
[13] Griffith AA. The phenomenon of rupture and flow in solids. Philos Trans R Soc 1920;A221:163–98.
[14] Suo Z, Ho S, Gong X. Notch ductile-to-brittle transition due to localized inelastic band. J Eng Mater Technol 1993;115:319–26.
[15] Li S, Thouless MD, Waas AM, Schroeder JA, Zavattieri PD. Mixed-mode cohesive-zone models for fracture of an adhesively bonded polymer–matrix composite. Eng Fract Mech 2006;73:64–78.
[16] Sills RB, Thouless MD. The effect of cohesive-law parameters on mixed-mode fracture. Eng Fract Mech 2013;109:353–68.
[17] Needleman A. An analysis of tensile decohesion along an interface. J Mech Phys Solids 1990;38:289–324.
[18] Xu X -P, Needleman A. Void nucleation by inclusion debonding in a crystal matrix. Modelling Simulation Mater Sci Eng 1993;1:111–32.
[19] Goutianos S, Sørensen BF. Path dependence of truss-like mixed mode cohesive laws. Eng Fract Mech 2012;91:117–32.
[20] Sørensen BF, Gamstedt EK, Østergaard RC, Goutianos S. Micromechanical model of cross-over fibre bridging - prediction of mixed mode bridging laws. Mech Mater 2008;40:220–34.
[21] Van den Bosch MJ, Schreurs PJG, Geers MGD. An improved description of the exponential xu and needleman cohesive zone law for mixed-mode. Eng Fract Mech 2006;73:1220–34.
[22] Yang QD, Thouless MD. Mixed-mode fracture analyses of plastically-deforming adhesive joints. Int J Fract 2001;110:175–87.
[23] Rice JR. Mathematical analysis in the mechanics of fracture. In: Liebowitz H, editor. Fracture: An Advanced Treatise. 2, Mathematical Fundamentals, New York, NY, USA: Academic Press; 1968, p. 191–311.
[24] Thouless MD. Fracture of a model interface under mixed-mode loading. Acta Metall Mater 1990;38:1135–40.
[25] Liechti KM, Chai YS. Biaxial loading experiments for determining interfacial fracture-toughness. J Appl Mech Trans ASME 1991;58:680–7.
[26] Irwin GR. Analysis of stresses and strains near the end of a crack traversing a plate. J Appl Mech 1957;24:261–364.
[27] Parmigiani JP, Thouless MD. The effects of cohesive strength and toughness on mixed-mode delamination of beam-like geometries. Eng Fract Mech 2007;74:2675–99.
[28] Sills RB, Thouless MD. Cohesive-length scales for damage and toughening mechanisms. Int J Solids Struct 2015;55:32–43.
[29] Rice JR. A path independent integral and the approximate analysis of strain concentration by notches and cracks. J Appl Mech 1968;35:379–86.
[30] Sørensen BF, Kirkegaard P. Determination of mixed mode cohesive laws. Eng Fract Mech 2006;73:2642–61.
[31] Bao G, Suo Z. Remarks on crack-bridging concepts. Appl Mech Rev 1992;45:355–66.
[32] Conroy M, Kinloch AJ, Williams JG, Ivankovic A. Mixed mode partitioning of beam-like geometries: A damage dependent solution. Eng Fract Mech 2015;149:351–67.
[33] Rice JR. Elastic fracture concepts for interfacial cracks. J Appl Mech 1988;55:98–103.
[34] Svensson D, Alfredsson KS, Stigh U. On the ability of coupled mixed mode cohesive laws to conform to lefm for cracks in homogeneous orthotropic solids. Eng Fract Mech 2016;163:426–48.
[35] Conroy M. Mixed mode fracture in fibre reinforced polymer composites. Ph.D. thesis, University College Dublin, Dublin, Ireland; 2015.
[36] Thouless MD. Mixed-mode fracture of a lubricated interface. Acta Metall Mater 1992;40(6):1281–6.
[37] Charalambides M, Kinloch AJ, Wang Y, Williams JG. On the analysis of mixed-mode failure. Int J Fract 1992;54:269–91.
[38] Park K, Paulino GH, Roesler JR. A unified potential-based cohesive model of mixed-mode fracture. J Mech Phys Solids 2009;57:891–908.
[39] Spring DW, Daniel W, Giraldo-Londono O, Paulino GH. A study on the thermodynamic consistency of the park-Paulino-roesler (PPR) cohesive fracture model. Mech Res Commun 2016;78:100–9.
[40] Tvergaard V, Hutchinson JW. The influence of plasticity on mixed mode interface toughness. J Mech Phys Solids 1993;41:1119–35.
[41] Sørensen BF, Goutianos S. Mixed mode cohesive law with interface dilatation. Mech Mater 2014;70:76–93.
[42] Hutchinson JW, Suo Z. Mixed mode cracking in layered materials. In: Hutchinson JW, Wu TY, editors. Advances in Applied Mechanics. Advances in Applied Mechanics, 29, Academic Press Inc; 1992, p. 63–191.
[43] Macaulay WH. Note on the deflection of beams. In: Glaisher JWL, editor. Messenger of Mathematics. XLVIII, Bowes & Bowes, Cambridge, UK; 1919, p. 129–30.